

## Mechanism of electromagnetic emission in plastically deformed ionic crystals

V. Hadjicontis,<sup>1,\*</sup> C. Mavromatou,<sup>1</sup> T. N. Antsygina,<sup>2</sup> and K. A. Chishko<sup>2</sup>

<sup>1</sup>*Department of Solid State Physics, University of Athens, Panepistimiopolis, Zografos, TK 157 84, Athens, Greece*

<sup>2</sup>*B. Verkin Institute for Low Temperature Physics and Engineering, 47 Lenin Avenue, 61103 Kharkov, Ukraine*

(Received 13 February 2007; revised manuscript received 30 May 2007; published 12 July 2007)

Experiments on the plastic deformation of LiF ionic monocrystals under uniaxial compression are performed with simultaneous recording of acoustic (AE) and electromagnetic (EME) emissions. A strong correlation between AE and EME events has been found, which clearly demonstrates that the observed EME is caused by a dynamical interaction between moving dislocations and charged vacancies in the ionic lattice during work hardening. The mechanism proposed to explain EME is based on the assumption that gliding edge dislocations sweep up the vacancies of a preferable sign. As a result, when a dislocation pileup is formed, a certain nonequilibrium charge density is accumulated at its head, resulting in electric polarization of the deformed crystal. As the external loading increases, a locked dislocation pileup bursts through the stoppers and quickly loses its bounded charge. The relaxation of this charge produces an intrinsic polarization current generating an electric pulse. It is assumed that the relaxation current can be described as an athermal viscous motion of vacancies under the kinetic friction force  $\sim Bv$  ( $B$  is the friction coefficient and  $v$  is the vacancy velocity) in a self-consistent electric field determined by the distribution of the total charge density. A nonlinear integro-differential equation of motion for the nonequilibrium charge density is derived. For a special form of the initial charge density distribution, an automodel solution of this equation describing the polarization current has been built. The electrical signal generated by an acting slip system has been calculated. By comparing the calculated and experimentally measured electric signal patterns, the friction coefficient for the linear chain of vacancies (the analog of an edge dislocation extra plane) in LiF has been estimated to be  $B \approx 0.9 \times 10^{-5} \text{ g cm}^{-1} \text{ s}^{-1}$ . This value is in accordance with the corresponding coefficient for dislocations in ionic lattices.

DOI: [10.1103/PhysRevB.76.024106](https://doi.org/10.1103/PhysRevB.76.024106)

PACS number(s): 62.20.Fe, 61.72.-y, 77.22.Ej

### I. INTRODUCTION

The deformation and destruction of solids are accompanied by lattice excitations which, in their turn, disturb the local equilibrium charge density in the electron-ionic subsystem of the crystal. Thus, the dynamic deformation is accompanied by the generation of both elastic and electromagnetic fields. Macroscopic lattice excitations of deformed crystalline media known as acoustic emission (AE) have been intensively studied over the last 70 years both experimentally and theoretically.<sup>1-7</sup> The great interest in this phenomenon can be explained by its wide application in material sciences<sup>8</sup> as well as by the intention to investigate the fundamental physical mechanisms responsible for the AE formation in real crystals.<sup>9-12</sup> Until now, it has been well established that the observable AE is caused by dynamical processes associated with nucleation, motion, and emergence on the crystal surfaces of large dislocation groups and regular dislocation pileups (such as slip bands and cracks). The corresponding AE mechanisms can be described successfully within a universal approach based on the dynamic theory of dislocations.<sup>13-15</sup>

The nature of electromagnetic events during the plastic deformation and fracture of nonpiezoelectric crystals has been studied much less than AE despite the fact that the electrodeformation phenomenon known as the Stepanov effect was discovered in 1933.<sup>16,17</sup> The main part of the experimental research in this area concerned the static stress-induced polarization in ionic crystals under loading<sup>18-32</sup> or electrification after splitting, as well as crack

propagation.<sup>33-35</sup> Besides static effects, time-dependent polarization and charge redistribution during plastic deformation of ionic crystals were reported in a number of publications.<sup>18</sup> Stress-induced macroscopic transient electric currents were detected in compression tests,<sup>36</sup> under a stress gradient in indentation experiments,<sup>37,38</sup> as well as in bent crystals.<sup>39</sup> However, the aforementioned observations are, in fact, low-frequency quasistatic variations of polarization or charge density. They cannot be directly associated with dynamic deformation processes and interpreted as sources of electromagnetic irradiation from plastically deformed solids.

A systematic study of the physical processes responsible for the electromagnetic emission (EME) accompanying dynamic deformation and fracture of ionic crystals has been developed within the last two decades. This has particular practical importance since precursory signals have been experimentally observed before earthquakes.<sup>40-43</sup> As far as the laboratory investigation of high-frequency EME is concerned the following efforts have been carried out. Specifically in Ref. 44 a simultaneous registration of the intensity (count rate) of both acoustic and electromagnetic emissions was made. In Ref. 45 the relationship between EME parameters and specific peculiarities of a deformed ionic sample (in particular, type of impurities and their concentration) was discussed. In Ref. 46 the electromagnetic emission during crack opening in an ionic crystal was studied. In a set of experiments,<sup>47-50</sup> using high-resolution recording equipment, simultaneous registration of AE and EME was performed on LiF samples under uniaxial compression with a relatively high deformation rate. So it was made possible not only to record the pattern of individual EME pulses<sup>48</sup> but also to

detect each acoustic pulse corresponding to a given electromagnetic event.<sup>47–50</sup> Thus, it was experimentally proved that the same dynamic structure transformations are sources of both observed EME and AE.

Concerning the theory of electromagnetic effects in non-piezoelectric solids, there exist solved problems on the electrodynamics of phonon excitations in ionic crystals<sup>51,52</sup> and metals.<sup>53</sup> The problem of the interaction between dislocations and conduction electrons has also been studied for its role in the plasticity of normal metals and superconductors.<sup>54</sup> The influence of external fields on the dislocation mobility has been investigated in Refs. 18 and 55–57. However, the inverse problem—namely, the mechanisms of electromagnetic field generation during plastic deformation—is yet imperfectly understood. This is due to the specific nature of the problem. It is impossible to create a certain universal approach to solve it. Indeed, the success in a description of AE mechanisms was achieved when all the problems concerning AE were reduced to the general problem of macroscopic elasticity with moving dislocations as elastic field sources (continuum theory of dislocations).<sup>13–15</sup> As a result, in order to interpret a certain AE mechanism it is necessary to assign the distribution of dislocation currents to the given deformation process correctly<sup>4,5,7,10</sup> and then to calculate the sound fields generated by dislocations.<sup>4,7,58</sup>

In contrast to AE, electromagnetic emission is caused not only by the distribution of dislocation currents but also by real mechanisms of the interaction between dislocations and charge carriers.<sup>18</sup> Of course, both the nature of the interaction and type of charge relaxation mechanisms are quite different in ionic insulators, conductors, semiconductors, and superconductors. Thus, first, the dislocation currents corresponding to a given deformation process should be determined and, second, the problem of the charge redistribution forced by moving dislocations should be formulated and solved. Then the corresponding electromagnetic fields can be obtained.<sup>59</sup>

As applied to the plasticity of ionic crystals, the above-described scheme has to include the known mechanism of the interaction between dislocations and charged vacancies or impurities. The dislocations move under external stress and involve bonded charges in the motion. Consequently, mobile dislocations act as electromotive forces transporting charge through the ionic lattice. The properties of these forces are determined by vacancy (or impurity) localization-delocalization processes on mobile dislocations. A plausible mechanism of the formation of polarization currents due to the interaction between a dislocation and its vacancy atmosphere was discussed in Refs. 60–63. In Ref. 64 a thermodynamic approach was proposed to explain the correlation between EME activity and point defect parameters in NaCl.

In the present work we develop a physical model for the generation of pulselike electric signals in ionic crystals under loading. The model is based on the relaxation of nonequilibrium charge density produced in the vacancy subsystem by dynamic dislocation currents of a plastically deformed ionic lattice. The obtained theoretical results are used to interpret the experimental data of simultaneously registered AE and EME from deformed LiF monocrystals. In Sec. II, we present the experimental results on AE and EME registration

in LiF monocrystals under uniaxial compression. In Sec. III, we propose and justify the model for the formation of intrinsic polarization currents caused by interaction between moving dislocations and charged vacancies. In Sec. IV, we introduce the equation of motion for a nonequilibrium vacancy charge density produced by mobile dislocations. In Sec. V, an automodel solution of this equation is acquired, and in Sec. VI, the electric pulse generated by an active slip plane is calculated. Section VII contains the discussion and comparison between the theory and experiment. Here we do not discuss any effects associated with the deformation of piezoelectrics. One of the most practically important kind of solids, where piezoelectricity is the main mechanism of EME during deformation and destruction, are the natural rocks (e.g., granites). Structurally, they are polycrystalline composites containing piezoelectric inclusions. Both their mechanical properties and the mechanisms responsible for the electromagnetic emission under loading differ substantially from those in ionic insulators or metals. The problem of EME in piezoelectrics (with applications to the natural rocks) will be a topic of a special publication in the near future. Within the last two decades diagnostic methods based on the registration of the electromagnetic emission from the Earth crust have been widely applied in geophysics, especially for the prediction of earthquakes and other disastrous events.<sup>40–43,65–68</sup> All the geoelectric and geomagnetic variations observed worldwide are, in fact, due to macroscopic deformation processes in the stressed crust materials. So the results of the present work are expected to be useful for the proper understanding of the physical processes responsible for the creation of geoelectromagnetic signals. Undoubtedly, investigations of the elementary dislocation mechanisms of electromagnetic field generation in solids are of great importance for the future progress of geosciences and materials engineering.

## II. EXPERIMENTS

Experiments on the uniaxial compression of LiF monocrystals were performed in order to investigate the various features of the EME generation processes during plastic deformation and destruction of ionic lattices. Specimens of size approximately  $0.5 \times 0.5 \times 1 \text{ cm}^3$  were cut along [100], [010], and [001] directions from LiF monocrystals. The content of the divalent cation impurities in different samples was estimated in the range 25–35 ppm (by weight). No special treatment of the crystal surface (like mechanical or chemical polishing, etc.) was made.

### A. Experimental setup

The mechanic and electronic instrumentation setup for simultaneous EME and AE detection along with the loading curve has been designed and built in the Solid State Laboratory of Athens University.<sup>47–50,61–63,71,72</sup> The complete system consists of two main parts: the mechanical part, incorporated for the uniaxial compression of the crystal and the detection part, which includes the electronics which can be altered in accordance with the requirements of the particular experi-

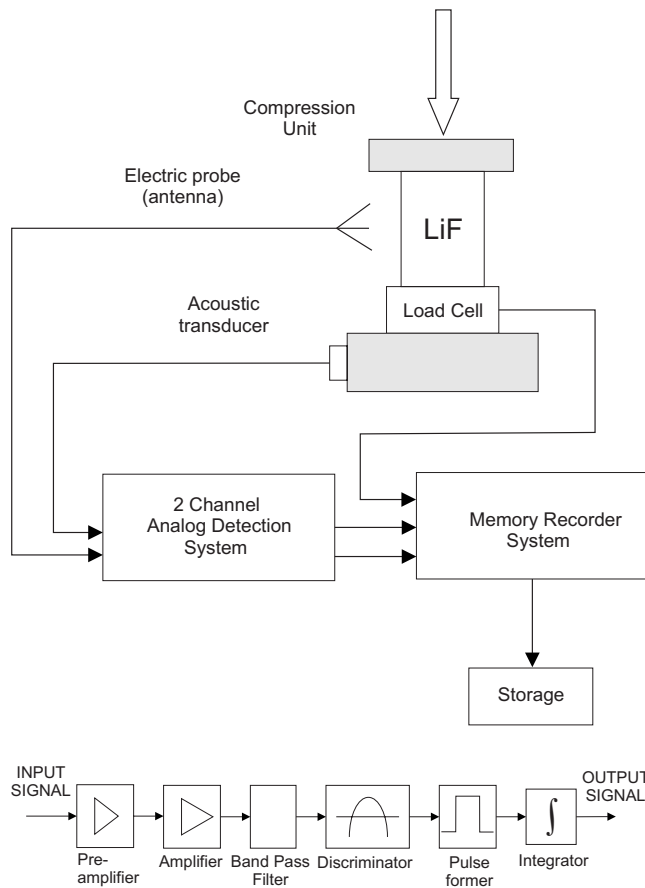


FIG. 1. (a) Experimental setup for the recording of the EME and AE count rate along loading until the failure of the sample. (b) Block diagram of the analog detection system (one channel).

ment. The mechanical compression unit is a nonelectrical hand-operated hydraulic machine, which makes it possible to avoid an interference from self-induced electric noise. The external loading is measured by the loading cell. The acoustic transducer (piezoelectric) is mounted at the base on which the sample stands. In order to eliminate external electric noises the entire experimental setup as well as the manipulator is placed in an earthed shielded room (Faraday cage) made of copper foil.

Four types of experiments were carried out.

(i) Simultaneous recording of the count rate (pulses/s) of both the AE (via a mechanoelectric transducer) and EME (via a simple monopole wideband antenna) as is shown in Fig. 1(a). The load on the sample gradually increases at a relatively constant rate, and the sample gradually deforms until its failure. The analog device consists of two identical channels (correspondingly for AE and EME signals) with a frequency range from 10 Hz up to 1 MHz. Each channel [Fig. 1(b)] includes the input preamplifier, an appropriate bandpass filter, and an amplifier followed by a discriminator with a pulse-forming circuit. The produced pulses are collected by an integrator, and the output signal is fed to a memory recorder (MR) HIOKI 8185. The output signal depicts the count rate (counts per second), which is digitally recorded by the MR. The sampling rate in this case is relatively low, up to 100 samples/s.

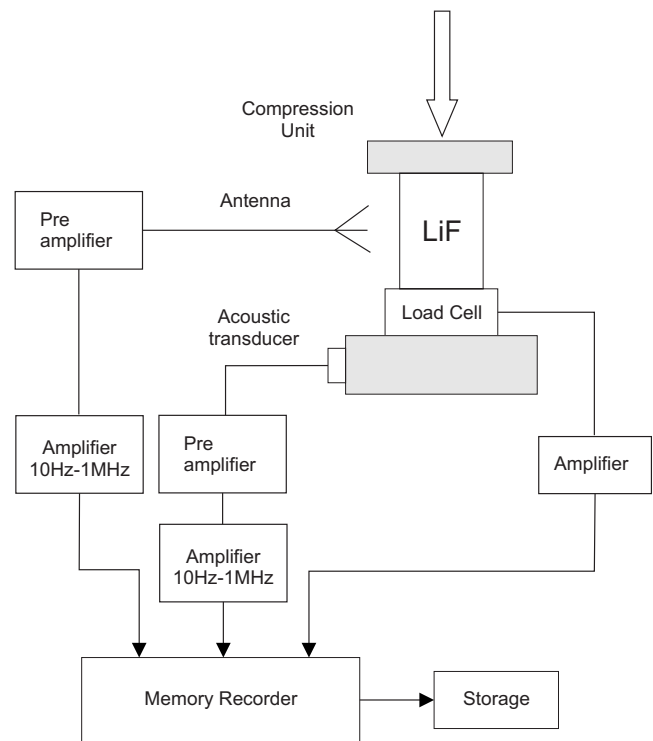


FIG. 2. Experimental setup for the recording of real-time series of the acoustic and electromagnetic pulses along loading.

(ii) Simultaneous detection and recording of the real-time series of acoustic and electromagnetic pulses (Fig. 2). The load on the sample gradually increases with a relatively constant rate, and the sample gradually deforms until failure. The electric field variations around the sample are transduced by the monopole antenna. The analog output signals (AE and EME) are fed to the channels of the digital memory recorder HIOKI 8185. The maximum sampling rate in this case is 1 Msample/s.

(iii) Detection of the stress-induced polarization currents via a silver electrode painted on the sample surface. The electric signal is amplified by a single-ended electrometer amplifier with input resistance up to  $10^{13} \Omega$ , as indicated in Fig. 3. The input is grounded through a resistor  $R = 100 \text{ M}\Omega$ . The charge separation and redistribution take place in the bulk of the sample under loading, which results in a macroscopic polarization of the sample and, thus, in a variation of the electric field around the sample. Consequently, the potential of the painted electrode (with reference to the ground) temporarily changes. A stress-induced transient current (polarization current) flows in order to compensate this potential difference. The time constant of the input circuit is mainly determined by the nominal value of the resistor  $R$ .

(iv) Simultaneous capture and recording of individual acoustic and electromagnetic pulses corresponding to a separate microfracture event. These pulses are recorded using a transient digital recording system with the same experimental setup as in case (ii), with internal triggering. Because of the extremely short duration of those individual pulses, the sampling rate for their recording is 1 Msample/s (transient recorder).

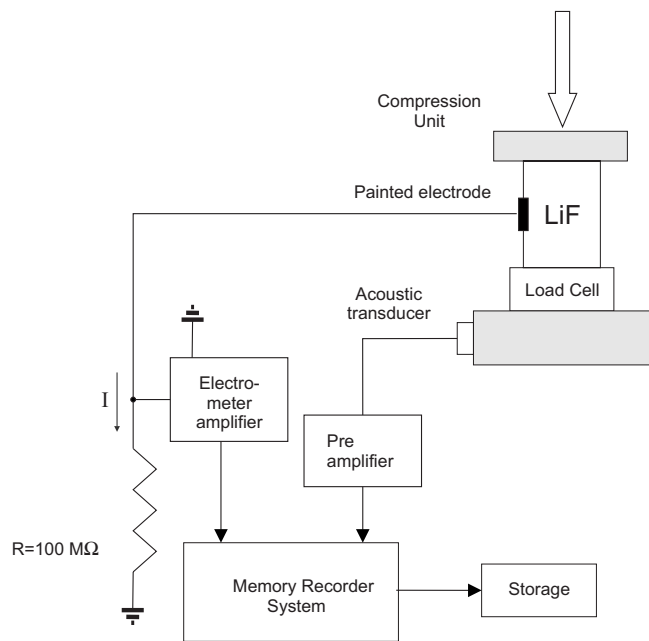


FIG. 3. Experimental setup for the recording of the low-frequency stress-induced polarization current in the LiF crystals under loading-unloading treatment up to the failure. The AE is registered simultaneously as the real-time series.

### B. Experimental results

Figure 4 demonstrates the count rate of acoustic [Fig. 4(b)] and electromagnetic [Fig. 4(c)] pulses whose amplitudes are above the noise level. The data are plotted along with the loading curve [Fig. 4(a)]. The experiment was performed using experimental procedure (i). The strain rate of the deformation is  $\dot{\epsilon} \sim 0.5 \times 10^{-3} \text{ s}^{-1}$ . The estimated yield point (resolved shear stress) for our LiF samples is  $\sigma_0 \sim 3.35 \pm 0.2 \text{ MPa}$  and agrees closely with the data in Refs. 69–72 and other literature sources.<sup>73</sup> This experimental value is quite consistent with that derived from the well-known dependence of  $\sigma_0$  on  $\dot{\epsilon}$ .<sup>69</sup>

It is evident from Figs. 4(b) and 4(c) that AE and EME distributions along the loading curve are quite similar in general but different in details. Both AE and EME appear at the deformation stress  $\sigma > \sigma_0$ . As the work hardening develops, both emissions become more active and reach their maximum intensities in the predestruction region. This means that the physical reasons for both emissions are the same. AE is known to be caused by dynamical dislocation processes (nonuniform motion, multiplication and annihilation of dislocations, dislocation reactions, and fatigue destruction at a late stage of deformation) accompanying the plastic deformation of a crystal. Thus, it is clear that EME as well as AE is due to the evolution of the dislocation structure. The results shown in Fig. 4 are in agreement with the corresponding observations of Ref. 44.

As can be seen from Fig. 4, at all deformation stages EME is more pronounced but at the easy glide stage (between the 10th and 30th seconds of the deformation) AE and EME differ most substantially. At this stage EME displays a lot of high-amplitude peaks whereas AE shows only several

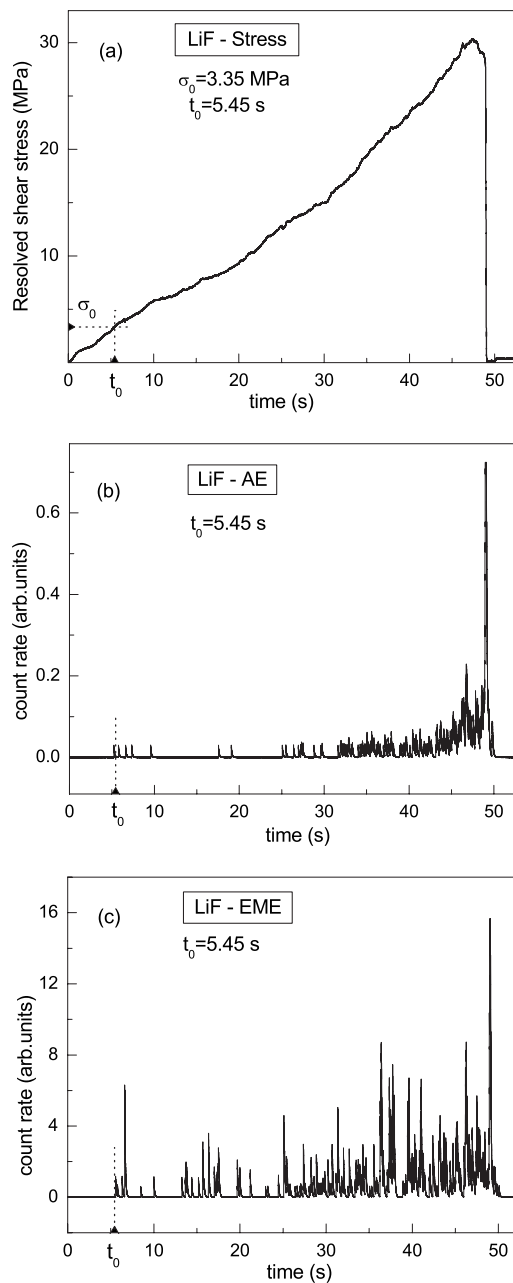


FIG. 4. Loading curve (a) with acoustic (b) and electromagnetic (c) emission intensities of the plastically deformed LiF crystal vs time. Count rates for AE and EME are given in arbitrary units. The measurement circuit is shown in Fig. 1.

small events. Such behavior is quite clear. Indeed, the easy glide consists in the motion of separate dislocations through the net of point obstacles, and this motion produces the low-amplitude high-frequency acoustic noise. On the other hand, even a separate dislocation when moving in an ionic lattice is able to accumulate an essential charge.<sup>18</sup> As a result, a separate dislocation or a small dislocation group can generate a noticeable polarization current. At the work hardening stage when large dislocation pileups are involved in the plastic flow both AE and EME grow up essentially.

The results of simultaneous measurements of real-time AE and EME signals obtained using experimental procedure

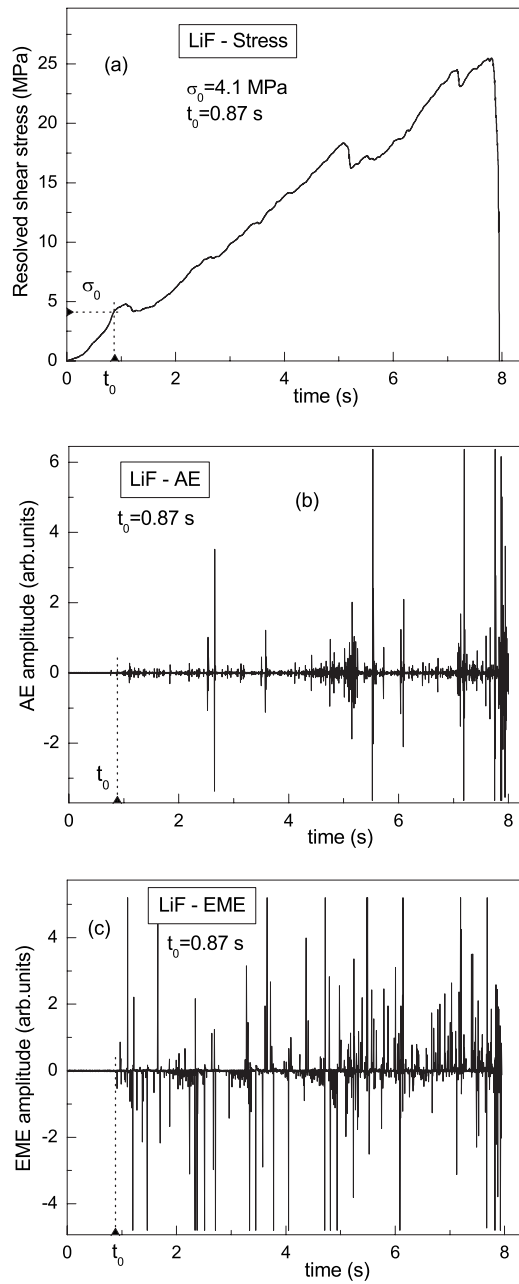


FIG. 5. The loading curve (a) and electromagnetic (b) and acoustic (c) emissions from LiF deformed with the strain rate  $\dot{\epsilon} \sim 10^{-2} \text{ s}^{-1}$ . The emission amplitude is given in a voltage recalculated to the input of the preamplifiers. The measurement circuit is shown in Fig. 2.

(iii) for the LiF monocrystal deformed with relatively high strain rate ( $\dot{\epsilon} \sim 10^{-2} \text{ s}^{-1}$ ) are shown in Fig. 5. The yield point in this case is  $\sigma_0 \sim 4.1 \pm 0.2 \text{ MPa}$  [Fig. 5(a)] which is in agreement with the dependence of  $\sigma_0$  on  $\dot{\epsilon}$ .<sup>69</sup> As before, at the easy glide stage EME [Fig. 5(c)] is more active than AE [Fig. 5(b)]. Besides, it is seen that significant bursts of AE accompany the evident jumps of the loading stress.

The Kaiser effect is known to be direct evidence of the dislocation nature of AE and EME in crystals.<sup>45,50</sup> In the present work using experimental procedure (ii) we investigated the Kaiser effect on LiF monocrystals by measuring

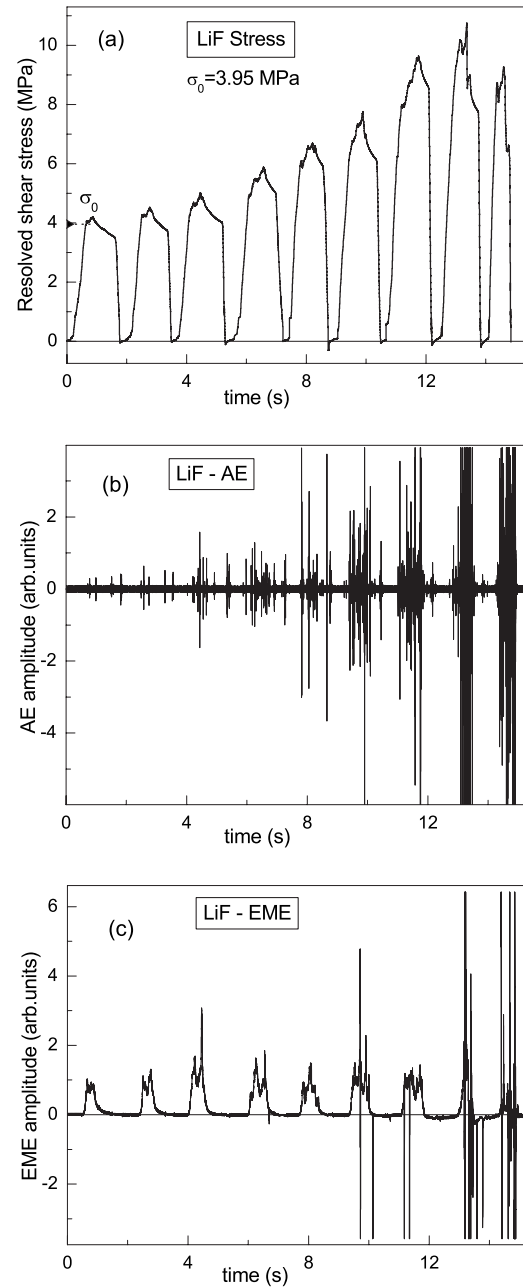


FIG. 6. Kaiser effect on the uniaxially deformed LiF: (a) is the loading curve. The magnitudes of acoustic emission (b) and low-frequency electric signal (c) are given in voltage recalculated to the input of the preamplifiers. The measurement circuit is shown in Fig. 3.

the low-frequency EME along with registration of the real-time AE signal. The results obtained are shown in Fig. 6. In this experiment the primary value of  $\sigma_0$  [Fig. 6(a)] is  $3.95 \pm 0.2 \text{ MPa}$ . It is seen that the EME signal occurs at the moment when the deforming stress attains the yield point  $\sigma_0$  [Fig. 6(a)]. This means that the electrical polarization of the crystal is caused by the dislocation slip. Within the first loading cycle just above the yield point there exist some electrical pulses up to the loading drop. In all subsequent cycles the emission reappears at the loading level at which it stopped in

the previous cycle. It can be seen from Fig. 6 that in the second and third cycles this level exceeds the yield point only slightly. Thus, we can conclude that the first three cycles refer to the easy glide stage. At the same time the amplitudes of the electrical signals increase from the first to the third cycle. This means that there are no essential hindrances to prevent the dislocation motion, but the number of dislocations increases due to multiplication and stable slip bands are formed. Comparing AE and EME at the easy glide stage we can state that EME is more pronounced than it was in the previous case (Fig. 4).

Beginning with the fourth cycle, the level of external stress corresponding to restoration of the plastic flow increases more rapidly, which is an indication of the work hardening stage. Electrical signals become extremely irregular because of the quick dynamic dislocation processes leading to the formation, breaking through and emerging on the crystal surface of the great dislocation pileups. In the sixth and seventh cycles, individual narrow high-amplitude electrical bursts appear, which might correspond either to the emergence of large dislocation pileups on the external surface or to the nucleation of fatigue cracks. Finally, in the eighth and ninth loading cycles the electrical signal consists of a dense sequence of high-amplitude peaks of different polarity. This picture is characteristic of the predestruction stage when fatigue cracks actively form and develop.

The AE behavior corresponds to the traditional picture as well. At the easy glide stage AE is a high-frequency noise with rare separate short pulses of high amplitudes exceeding the noise level. In the work hardening regime the AE pattern is enriched: the number of pulses exceeding the noise threshold increases. From the fifth cycle AE has the form of dense packs consisting of short high-amplitude pulses. These packs exist just within the loading period. At the predestruction stage AE is catastrophic in character. Noticeable AE signals also occur in the unloading periods, which points to the fact that the mechanical relaxation process continues after removing the external stress.

Our main goal is to study the correlation between acoustic and electromagnetic emissions. At the easy glide stage the AE pulses with amplitudes higher than the noise threshold appear in intervals where the electrical signal is rather irregular. The electrical burst in the third cycle is accompanied by a pack of acoustical pulses. A distinct correlation between amplitudes and spectral compositions of AE and EME is also observed in all other loading cycles. Thus, the present experimental investigation proves unambiguously that mechano-electrical effects in deformed LiF are associated with the interaction between mobile dislocations and lattice charges.

Figure 7 demonstrates the direct correlation between AE and EME. It shows a single electric pulse from the sequence of Fig. 5(b) and the AE signal from the sequence of Fig. 5(c) generated by one and the same elementary deformation event. The front of the acoustic signal lags behind the electric pulse by  $185 \mu\text{s}$  because of the finite time needed for the acoustic emission to reach the acoustic transducer. It is important to note that the electric signal has a simple definite form whereas the acoustic signal, being a composition of eigenexcitations of the finite-sized crystal,<sup>74</sup> consists of a great number of fast oscillations. This means that in compari-

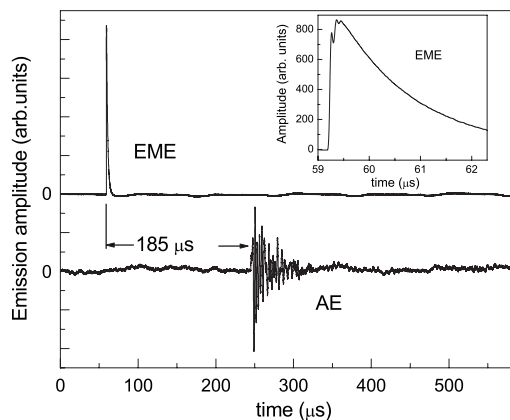


FIG. 7. Correlation between AE and EME: a single electric pulse and the corresponding acoustic signal. The delay of the acoustic pulse is equal to  $185 \mu\text{s}$ . The inset shows the shape of the EME pulse on an enlarged time scale.

son to AE the electrical sequence is much more informative in view of the identification of an individual deformation event. The inset in Fig. 7 presents the electric pulse on an enlarged time scale. It can be seen that the front of the pulse has an irregular shape and the period of oscillations near the top of the pulse is just equal to the sampling time ( $0.5 \mu\text{s}$ ) of the analog-digital transformer. It is a typical distortion of the short-time process reproduced by the digital transformer with the finite step of quantization. The transformation of such a kind distorts also the real pulse amplitude, reducing its value. The slow decreasing tail of the pulse is smooth, but its real-time run is distorted by the transfer function of the bandpass filter (substantially because of its lower cutoff frequency). We will take into account all the mentioned features in Sec. VII when comparing the theory and experiment.

The experiments described prove the connection between dynamic dislocation processes and the generation of electromagnetic emission in LiF crystals. In the following sections we propose a theoretical model in order to describe the phenomena under study.

### III. MODEL

The experimental results described in Sec. II show that a detectable electromagnetic emission is observed at the easy glide stage but it increases most substantially at the promoted stages of work hardening. The bursts of EME are often accompanied by visible jumps of the loading stress  $\sigma(t)$ . The occurrence of an EME individual pulse correlates with the jump of unloading in such a way that a separate short electromagnetic signal precedes the beginning of the stress discharge whereas the corresponding AE signal series appears after a lapse of time necessary for the acoustic response formation in the sample-basis system. This AE series is generated throughout the full jump duration up to restoration of the average loading level peculiar to the actual work hardening stage. It should be noted that separate AE pulses can often be registered from an unloaded sample (e.g., during a Kaiser effect investigation) due to residual relaxation in the

lattice defect substructure, whereas EME appears only because of an active deformation of the ionic crystal.

It is known that easy glide in crystals is associated with the progress of slip systems including the dislocation multiplication supported by the action of dislocation sources (e.g., Frank-Read sources, cross slip, etc.). As a rule, in cubic crystals of LiF type under uniaxial loading only two slip systems are activated.<sup>75</sup> While the deformation is in progress, these systems cross each other and the mobile dislocations come to a stop. Thus, we have the stage of work hardening when locked dislocation pileups are formed.

As the loading stress increases some of the locked pileups burst through their stoppers. Each burst leads to the quick emergence of the released slip band on the crystal surface. This process is accompanied by the strain jump (proportional to the total Burgers vector of the emerged dislocations) and the corresponding loading discharge. On far-promoted stages of deformation, the dislocation density becomes so high that all the pileups are locked strongly and the dislocations are unable to leave the crystal. As a result, a nucleation of fatigue cracks begins.

Here we are interested in mechanisms controlling the motion and redistribution of charge during plastic deformation of an ionic crystal. To develop the model for a description of the experimentally observable phenomena, as the first step, we restrict our consideration only to processes that occur in the subsystem of charged vacancies interacting with mobile dislocations.<sup>18-21</sup>

It is established experimentally that mobile edge dislocations in ionic lattices “sweep up” the charged vacancies which they meet on their way.<sup>18-21</sup> It means that the moving dislocations adsorb the vacancies, accumulating the charge in their cores and transferring it with the dislocation lines. It is a well-known effect of electric polarization in ionic crystals under loading.<sup>18</sup> If LiF crystals are grown without special precautions, they usually contain a noticeable amount of divalent cation impurities (typically,  $Mg^{2+}$ ) and, as a result, have an excessive density of negatively charged vacancies. Most of these vacancies are localized in vacancy-impurity pairs (VIPs). Since the ionic radius of the impurity differs from the cation radius of the native lattice, the impurity is a dilatation center and, hence, a pinning center for the dislocation. The dislocation pinned on such an impurity obstacle is also bounded with a vacancy of VIPs.

The crucial point of the picture discussed is as follows. When a dislocation unpins from an obstacle under external driving stress and moves to the next obstacle, it can catch the vacancy from the VIP and bound it in the dislocation core. Of course, this is possible at a certain relationship between the binding energies of VIP and vacancy-core complex. If the vacancy-core energy is high enough to bond the point defect, it will be caught by the passing dislocation. Naturally, under such conditions a portion of free (nonpaired) vacancies in the vicinity of the slip plane will be absorbed as well. The sign of the charge received by the mobile dislocation is determined by the predominant sign of vacancies near the slip plane. Cation impurities stimulate the excessive density of negatively charged vacancies in the lattice, which leads to a negative dislocation charge.<sup>18</sup> In contrast, mobile dislocations in anion-doped crystals with an excessive density of

positively charged vacancies are positively charged as follows from the experiment.<sup>22</sup>

However, mobile dislocations not only acquire the charge but also lose it.<sup>19,23-27</sup> The effects of losing are not studied in detail but it was shown that when dislocations move quickly or oscillate with a high frequency the loss increases. This is quite expected and is nothing more than a pinning and unpinning (and, hence, oscillating) of dislocation segments. The dislocation core is a potential hole for a vacancy, and core oscillations lead to an effective (parametric) decrease in the hole depth that makes easier a desorption of the bonded vacancy. Moreover, at accelerated dislocation motion there appears an inertia force acting on a bonded vacancy, and the higher the acceleration is (increasing with oscillation frequency), the more intensive is the force trying to desorb the vacancy.

We propose the following scheme for the EME formation during work hardening of the crystal. At the easy glide stage dislocations move in the slip planes picking up the charged vacancies. By the time the easy glide stage is finished the locked pileups have accumulated the vacancy charge mainly at their heads. This is because only leading dislocations of a slip system are able to trap most of the vacancies around the slip plane. At room temperature the thermodiffusion is negligible, so that there are no essential vacancy flows from the body of the crystal to the slip planes. Thus, only a limited amount of vacancies in the direct vicinity of the slip plane are accessible for absorption through barodiffusion caused by the stress field of mobile dislocations. By the promoted stage of work hardening there are a lot of locked pileups which have accumulated a considerable vacancy charge. Such a charge distribution is in nonequilibrium because it is produced by external work and in this connection the dislocation glide processes can be considered as an effective electromotive force stimulated by an external loading. As a result, an electric field produced by external sources appears in the crystal. On the other hand, the clouds of bonded vacancies are stoppers for dislocations along with dislocations from crossing slip systems, impurities, etc.

Finally, the pileups start bursting through under increasing loading. Every time the burst-through occurs, the bonded charge is released and the relaxation process brings the charge to equilibrium. The relaxation process means the appearance of polarization currents which will be described within our model.

The equation of motion for vacancies can be written as

$$\mu(\mathbf{r}, t) \frac{d\mathbf{v}(\mathbf{r}, t)}{dt} + B\mathbf{v}(\mathbf{r}, t) = \mathbf{f}(\mathbf{r}, t). \quad (1)$$

Here  $\mu(\mathbf{r}, t) = m[n^{(+)}(\mathbf{r}, t) + n^{(-)}(\mathbf{r}, t)]$  is the mass density of the total vacancy flow,  $n^{(\pm)}(\mathbf{r}, t)$  is the density (the number of carriers per unit volume) of positive and negative carriers, respectively, and  $m$  is the effective mass of carriers of the order of the ionic mass. For simplicity we assume that positive and negative carriers are of the same mass. The value  $\mathbf{v}(\mathbf{r}, t)$  is the velocity field of the vacancy flow,  $\mathbf{f}(\mathbf{r}, t)$  is the force density, and  $B$  is the coefficient of the viscous friction of the carriers. Equation (1) describes the force-driving mi-

gration of vacancies as an athermic process in a viscous medium. The viscosity is caused by a vacancy-phonon interaction. Such an approach is similar to that for dislocation dynamics in an elastic continuum. The volume density of electrostatic forces is

$$\mathbf{f}(\mathbf{r}, t) = \rho(\mathbf{r}, t) \int dV' \rho(\mathbf{r}', t) \frac{\mathbf{r} - \mathbf{r}'}{|\mathbf{r} - \mathbf{r}'|^3}, \quad (2)$$

where  $\rho(\mathbf{r}, t) = q[n^{(+)}(\mathbf{r}, t) - n^{(-)}(\mathbf{r}, t)]$  is the total charge density and  $q$  is the absolute value of a vacancy charge.

The equation of motion (1) must be supplied by the continuity equation

$$\frac{\partial \rho(\mathbf{r}, t)}{\partial t} + \text{div}[\rho(\mathbf{r}, t)\mathbf{v}(\mathbf{r}, t)] = 0, \quad (3)$$

as well as initial (and, if necessary, boundary) conditions. If all the conditions are given, then the set of equations (1)–(3) describes the relaxation kinetics of the nonequilibrium lattice charge distribution initially produced by a certain plastic deformation. As applied to a realistic situation, the treatment of Eqs. (1)–(3) will be considered in the next two sections.

#### IV. EQUATION OF MOTION FOR VACANCIES SWEEP UP FROM THE SLIP PLANE

The set (1)–(3) consists of nonlinear integro-differential equations, and its solution cannot be found in a general form. Here we treat these equations using qualitative analysis based on plausible physical speculations.

We employ the model of an isotropic continuum with shear modulus  $G$  and Poisson's ratio  $\nu$ . A slip plane  $z=0$  is created by a dislocation source located at  $x=0$ . The source produces rectilinear (parallel to the  $y$  axis) edge dislocations with Burgers vectors  $\mathbf{b}=(b, 0, 0)$ . At the work hardening stage the easy glide becomes slower and the leading dislocations are stopped on the obstacles, and as a result, a two-side dislocation pileup of  $2l_0$  length locked at  $x=\pm l_0$  is formed. Under these assumptions the dislocation density  $\rho_D$  in the pileup has the form<sup>75</sup>

$$\rho_D(x, z) = D \frac{x}{\sqrt{l_0^2 - x^2}} \delta(z), \quad (4)$$

where  $\delta(z)$  is Dirac delta function,

$$D = \frac{2(1 - \nu)\sigma}{Gb},$$

and  $\sigma$  is an external shear stress. The dislocation distribution within the pileup is demonstrated by curve 1 in Fig. 8.<sup>75</sup>

For simplicity, we suppose that the “quasifree” charge of an ionic lattice redistributed during plastic deformation consists only of negatively charged vacancies.<sup>18</sup> It means that  $n^{(+)}(\mathbf{r}, t)$  remains constant in all deformation and relaxation processes. In reality this situation can result from the nature of the dislocation-vacancy interaction in an ionic crystal. Indeed, the divalent impurities in the LiF lattice are both the stoppers (as dilatation centers) for individual dislocations and “centers of condensation” for charged vacancies screen-

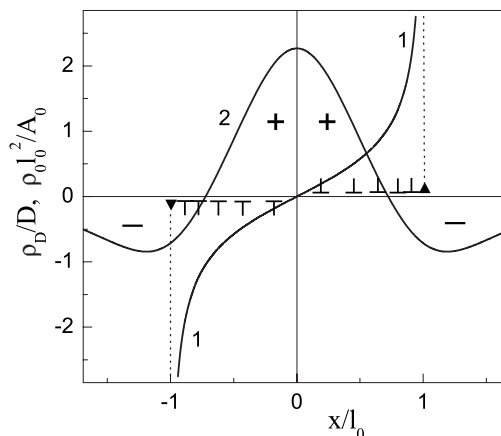


FIG. 8. The initial distribution of the charge (curve 2) bonded by the two-side dislocation pileup. Curve 1 is the dislocation density in the two-side pileup (Ref. 75).

ing the excessive impurity charge. As a result, most of excessive charged vacancies of the same sign are localized concurrently at both an impurity with the foreign valence and the dislocation line stopped at this impurity. Gliding through the lattice under an external stress, the dislocation overcomes impurity stoppers taking the screening charge because the vacancy-dislocation binding energy is greater than the corresponding value for VIPs. So the vacancy charge of a preferred sign will be swept by moving dislocations but the impurities remain immobile, having an unscreened charge of the opposite sign. This process is similar to charging of a capacitor through the work of electromotive forces.

The set of equations includes only the velocity of carriers and time or space derivatives of the charge density. The total density  $\rho(\mathbf{r}, t)$  is convenient to use as a principal variable for a description of the time-dependent relaxation processes. To build the necessary solution we need to know the initial non-equilibrium charge distribution  $\rho_0(x, z)$  at  $t=0$ . This initial distribution should be obtained as a solution of a separate complicated problem including the details of the vacancy-dislocation interaction and kinetics of vacancies supplied into the slip plane during the pileup formation. The solution of this problem is beyond the scope of the present paper. For our goal we use a plausible model which supposes that the vacancy charge is distributed uniformly along the infinite  $y$  axis ( $-L < y < L, L \rightarrow \infty$ ) and concentrated in the vicinity of the  $xy$  plane ( $|z| \leq \delta_0 \rightarrow 0$ , see Fig. 8),<sup>76</sup>

$$\rho(x, z, t) = \rho(x, t) \delta(z),$$

where

$$\rho(x, t) = A \left\{ \frac{2}{x^2 + \alpha^2} - \frac{1}{(x+l)^2 + \alpha^2} - \frac{1}{(x-l)^2 + \alpha^2} \right\}. \quad (5)$$

Here  $l$  is the half-length of a dislocation pileup,  $A$  is the amplitude of the vacancy charge distribution, and  $\alpha$  is the principal parameter determining the sharpness of the  $\rho(x, t)$  distribution. The parameters  $A$ ,  $\alpha$ , and  $l$  are, in general, time dependent. The distribution (5) satisfies the condition of electroneutrality,

$$\int_{-\infty}^{\infty} dx \rho(x, t) = 0, \quad (6)$$

which is the conservation law for the total charge during plastic deformation.

In view of Eq. (5), it is reasonable to assume that polarization currents produced due to the relaxation process are concentrated in the vicinity of the slip plane  $z=0$ , so that the equation of motion (1) with the initial condition  $\rho(x, t) = \rho_0(x)$  can be written as follows:

$$\mu(x, t) \frac{dv(x, t)}{dt} + Bv(x, t) = f(x, t), \quad (7)$$

where  $v(x, t)$  is the  $x$  component of the velocity field and  $f(x, t)$  is the  $x$  component of the driving force,

$$f(x, t) = 2\rho(x, t) \int_{-L}^L dx' \frac{\rho(x', t)}{x - x'}, \quad (8)$$

and  $2L$  is the crystal size along the  $x$  direction ( $L \rightarrow \infty$ ). The integral in Eq. (8) is treated as the principal value.

Let us take into account that at room temperature the carrier mobility under an external electric field is rather small<sup>77</sup> and has the character of viscous motion in the gas of lattice excitations (phonons). It is just the situation with the dislocation mobility in an ionic lattice.<sup>75</sup> It means that the inertial term in Eq. (7) is small as compared to the viscous force,  $\mu \ll Bt_R$ , where  $t_R$  is the characteristic relaxation time of essentially macroscopic value. As a result, the inertial term in Eq. (7) can be neglected, and we have

$$u(x, \tau) - \rho(x, \tau) \int_{-\infty}^{\infty} dx' \frac{\rho(x', \tau)}{x - x'} = 0. \quad (9)$$

Here

$$u(x, \tau) = \frac{B}{2} v(x, \tau), \quad \tau = \frac{2t}{B}, \quad (10)$$

where  $\tau$  is the renormalized time.

The continuity equation in the chosen geometry and new variables takes the form

$$\frac{\partial \rho(x, \tau)}{\partial \tau} + \frac{\partial}{\partial x} [\rho(x, \tau) u(x, \tau)] = 0. \quad (11)$$

The set of equations (9) and (11) at initial condition (5) makes it possible to describe the relaxation of a nonequilibrium charge produced during slip system activity in a plastically deformed ionic crystal.

## V. CHARGE RELAXATION

The system of nonlinear integro-differential equations (9) and (11) can be solved only by numerical methods. To estimate the characteristic time of the nonequilibrium charge relaxation we restrict our consideration to the qualitative analysis of  $\rho(x, \tau)$  behavior. For this purpose we employ the algorithm used in Ref. 78 to describe the evolution of curved dislocations with nonlocal self-action generated by the dynamic Frank-Read source.

The essence of the algorithm is as follows. The initial (at the moment  $\tau=0$ ) charge distribution (5) illustrated by curve 2 in Fig. 4 starts relaxing at  $\tau > 0$  until the equilibrium distribution  $[\rho(x, \tau)=0]$  is reached at  $\tau \rightarrow \infty$ . The relaxation is achieved by the flow of polarization currents. Let us suppose that the problem has an automodel solution  $\rho(x, \tau)$ , which at an arbitrary moment  $\tau$  can be described by a function of the form (5),

$$\rho(x, \tau) = A(\tau) \left\{ \frac{2}{x^2 + \alpha^2(\tau)} - \frac{1}{[x + l(\tau)]^2 + \alpha^2(\tau)} - \frac{1}{[x - l(\tau)]^2 + \alpha^2(\tau)} \right\}, \quad (12)$$

with parameters  $A(\tau)$ ,  $\alpha(\tau)$ , and  $l(\tau)$  determined within a relevant reiteration procedure at the initial conditions

$$A(0) = A_0, \quad \alpha(0) = \alpha_0, \quad l(0) = l_0. \quad (13)$$

The validity of the procedure will be established by direct verification within a durable iterative algorithm. Of course, the function (12) satisfies the condition (6) at arbitrary  $\tau$ .

Now, we describe the temporary evolution of the distribution  $\rho(x, \tau)$  within a time period  $\Delta\tau$  so small that the charge redistribution by the time  $\tau + \Delta\tau$  can be presented in the form

$$\rho(x, \tau + \Delta\tau) = \rho(x, \tau) + \rho'(x, \tau; \Delta\tau), \quad (14)$$

where  $\rho'(x, \tau; \Delta\tau)$  is considered as a function of  $\Delta\tau$  and  $x$ , and can be obtained as a solution of a linearized equation derived from Eqs. (9) and (11) on the assumption that  $\rho' \ll \rho$  (this condition can be satisfied by an appropriate choice of the time step  $\Delta\tau$ ).

First, let us estimate the integral in Eq. (9),

$$\int_{-L}^L \frac{dx'}{x - x'} [\rho(x', \tau) + \rho'(x', \tau; \Delta\tau)] \approx \Phi(x, \tau) + \rho'(x, \tau; \Delta\tau) \ln \frac{L+x}{L-x}, \quad (15)$$

where

$$\Phi(x, \tau) = \frac{\pi A(\tau)}{\alpha(\tau)} \left\{ \frac{2x}{x^2 + \alpha^2(\tau)} - \frac{x + l(\tau)}{[x + l(\tau)]^2 + \alpha^2(\tau)} - \frac{x - l(\tau)}{[x - l(\tau)]^2 + \alpha^2(\tau)} \right\} \quad (16)$$

and the second term in (15) can be omitted with logarithmic accuracy at  $L \rightarrow \infty$ . So the flow velocity has the form

$$u(x, \tau + \Delta\tau) = [\rho(x, \tau) + \rho'(x, \tau; \Delta\tau)] \Phi(x, \tau). \quad (17)$$

Substituting Eq. (17) into Eq. (11) one can obtain the quasi-linear equation

$$\begin{aligned}
 & \frac{\partial \rho'(x, \tau; \Delta \tau)}{\partial (\Delta \tau)} + 2\rho(x, \tau)\Phi(x, \tau) \frac{\partial \rho'(x, \tau; \Delta \tau)}{\partial x} \\
 & + 2\rho'(x, \tau; \Delta \tau) \frac{\partial}{\partial x} [\rho(x, \tau)\Phi(x, \tau)] + \frac{\partial}{\partial x} [\rho^2(x, \tau)\Phi(x, \tau)] \\
 & = 0,
 \end{aligned} \tag{18}$$

equivalent to two differential equations<sup>79</sup>

$$\begin{aligned}
 d(\Delta \tau) &= \frac{dx}{2u(x, \tau)} \\
 &= - \frac{d\rho'(x, \tau; \Delta \tau)}{\frac{\partial}{\partial x} [\rho(x, \tau)u(x, \tau)] + 2 \frac{\partial u(x, \tau)}{\partial x} \rho'(x, \tau; \Delta \tau)}.
 \end{aligned} \tag{19}$$

Finally, we have

$$\begin{aligned}
 \rho'(x, \tau; \Delta \tau) &= \frac{1}{2} \left( \frac{\partial u(x, \tau)}{\partial x} \right)^{-1} \\
 & \times \left[ \exp \left( 2\Delta \tau \frac{\partial u(x, \tau)}{\partial x} \right) - 1 \right] \frac{\partial}{\partial x} [\rho(x, \tau)u(x, \tau)].
 \end{aligned} \tag{20}$$

The value of  $\rho'$  is prescribed to the point  $x+\Delta x$ , where

$$\Delta x \approx 2u(x, \tau)\Delta \tau, \tag{21}$$

as follows from the first equation of the system (19) with regard to the smallness of the time step  $\Delta \tau$ .

With the help of the solution (20) we find the charge distribution (14) at  $\tau+\Delta \tau$  and then approximate it by the functional dependence (12) using the least-squares algorithm. As a result of this approximation we obtain new values for the parameters  $A(\tau+\Delta \tau)$ ,  $\alpha(\tau+\Delta \tau)$ , and  $l(\tau+\Delta \tau)$ . Then we repeat the procedure described on successive time steps to find the distribution at the moments  $\tau+2\Delta \tau$ ,  $\tau+3\Delta \tau, \dots$ , and so on up to the end of the desirable range of time variation. The stability and validity criteria of the algorithm consist in the fact that the found dependences  $A(\tau)$ ,  $\alpha(\tau)$ , and  $l(\tau)$  are continuous and smooth functions of the renormalized time  $\tau$  on the half-axis  $0 < \tau < \infty$  and obey the initial conditions (13). Besides, the additional conditions  $\alpha(\tau) \rightarrow 0$  at  $\tau \rightarrow \infty$  and  $A(\tau) \leq A_0$  at  $0 < \tau < \infty$  should be satisfied.

Now we calculate the relaxation of the distribution (12) for the case when  $l_0$  is constant equal to unity, the parameter  $A_0$  takes the fixed value from an interval  $0.5 < A_0 < 5.0$ , and only the parameter  $\alpha(\tau)$  is time dependent. The choice of  $l_0=1$  means that all length parameters are measured in units of  $l_0$ . The initial value of  $\alpha_0$  is taken from the region  $0.5 < \alpha_0 < 1.0$ . Figure 9 shows the results of the calculations. Figure 9(a) presents the dependences  $\alpha(\tau)$  for fixed  $\alpha_0=0.65$  at different  $A_0$ . Figure 9(b) demonstrates the dependences  $\alpha(\tau)$  for fixed  $A_0=1.0$  at different  $\alpha_0$ . In Fig. 9(c) the curves of Fig. 9(a) are replotted in a double-logarithmic scale. As can be seen, all the dependences  $\alpha(\tau)$ , irrespective of the initial values of  $\alpha_0$ , display a universal powerlike

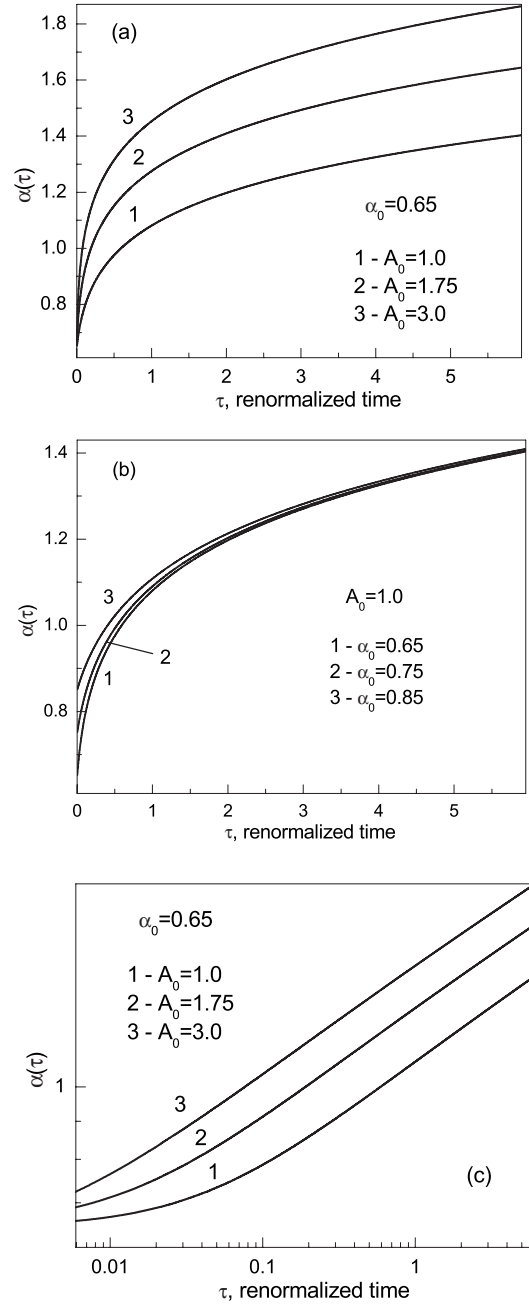


FIG. 9. Dependences  $\alpha(\tau)$ : (a) at different  $A_0$  and fixed  $\alpha_0$ , (b) at different  $\alpha_0$  and fixed  $A_0$ , and (c) curves from (a) on a double-logarithmic scale.

asymptotic behavior. This numerical result proves the validity of the representation for  $\rho(x, \tau)$  as automodel function (12).

The analysis of the dependences depicted in Fig. 9 shows that within the intervals of initial values  $0.5 < A_0 < 5.0$  and  $0.5 < \alpha_0 < 1.0$  the function  $\alpha(\tau)$  can be approximated by the following analytical expression:

$$\alpha(\tau) = \left\{ \alpha_0^7 + \frac{9}{5} A_0^\beta \tau \right\}^{1/7}, \quad \beta = \left( \frac{7}{5} \right)^2. \tag{22}$$

## VI. ELECTRIC PULSE

The results of Sec. V enable us to calculate the shape of the electric pulses generated due to the relaxation of the charge swept up and accumulated during the dislocation slip process. The relaxation begins when the locked dislocation pileup stimulated by the increasing external load bursts through the stoppers. The dislocations are accelerated on their way to the crystal surface. The vacancies bonded on dislocations begin shaking off, and this process takes place in a short but finite time interval. Formally, this fact can be included in the model developed in the previous sections if we assume that the charge involved in the relaxation,  $\rho_0(x, \tau)$ , grows from zero at the moment  $\tau=0$  when the acceleration begins up to the value

$$\rho_0(x) = A_0 \left\{ \frac{2}{x^2 + \alpha_0^2} - \frac{1}{(x + l_0)^2 + \alpha_0^2} - \frac{1}{(x - l_0)^2 + \alpha_0^2} \right\}, \quad (23)$$

within a period which is so short that the parameters  $\alpha(\tau) \approx \alpha_0$  and  $l(\tau) \approx l_0$  can be considered as practically unchanged. The corresponding process can be described by the time-dependent amplitude  $A(\tau)$  in  $\rho_0(x, \tau)$  with constant  $\alpha_0$  and  $l_0$ .

The real delocalization kinetics of the bounded charge during the accelerated motion of lattice dislocations is still an unsolved problem. Here, in order to describe the situation on a simple quantitative level we exploit the following reasonable assumptions. Let  $\rho_l(x, \tau)$  be the charge trapped by dislocation pileup,

$$\rho_l(x, \tau) = A(\tau) \left\{ \frac{2}{x^2 + \alpha_0^2} - \frac{1}{(x + l_0)^2 + \alpha_0^2} - \frac{1}{(x - l_0)^2 + \alpha_0^2} \right\}, \quad (24)$$

and  $\rho_l(x, 0) = \rho_0(x)$ . We suppose that the relative portion of the trapped vacancy charge lost by accelerated dislocation (the partial charge involved into relaxation) per unit time is proportional to the dislocation velocity. Thus, the charge loss is determined by the relation

$$\frac{1}{\rho_l(x, \tau)} \frac{\partial \rho_l(x, \tau)}{\partial \tau} = \frac{1}{A(\tau)} \frac{dA(\tau)}{d\tau} = -2\gamma\tau. \quad (25)$$

Here  $\gamma$  is a constant proportional to the dislocation acceleration (which is supposed to be constant). The value of  $\gamma$  is also determined by the coupling energy between the dislocation and charged vacancies. The trapped charge decreases with time according to the time dependence of  $A(\tau)$ ,

$$A(\tau) = A_0 \exp(-\gamma\tau^2). \quad (26)$$

Finally, the charge involved in relaxation is

$$\begin{aligned} \rho_0(x, \tau) &= \rho_0(x) - \rho_l(x, \tau) \\ &= A_0 [1 - \exp(-\gamma\tau^2)] \left\{ \frac{2}{x^2 + \alpha^2(\tau)} - \frac{1}{(x + l_0)^2 + \alpha^2(\tau)} \right. \\ &\quad \left. - \frac{1}{(x - l_0)^2 + \alpha^2(\tau)} \right\}. \end{aligned} \quad (27)$$

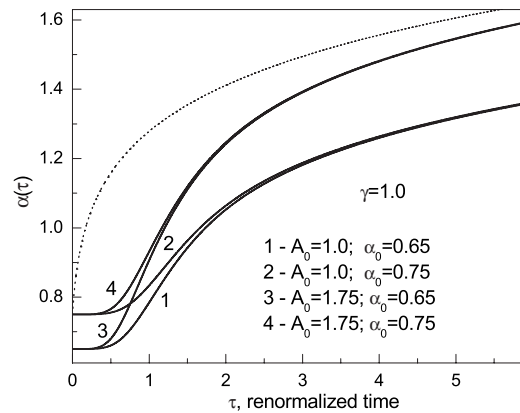


FIG. 10. Dependences  $\alpha(\tau)$  at different  $\alpha_0$  and  $A_0$ . The dotted line is curve 2 from Fig. 9(a).

The parameter  $l(\tau)$  is taken to be equal to  $l_0$  in the same manner as it was made in Sec. V. The amplitude of the distribution (27) becomes nearly equal to  $A_0$  in a time of the order of  $\sim 1/\sqrt{\gamma}$ . According to the assumption about the character of charge loss made after Eq. (23) the quantity  $\gamma$  has to satisfy the inequality

$$\frac{d\alpha(\tau)}{d\tau} \ll \sqrt{\gamma}\alpha(\tau). \quad (28)$$

The parameter  $\alpha(\tau)$  in Eq. (12) has to be fitted at every single moment  $\tau$  according to the actual value of  $\rho_0(x, \tau)$ . It means that the calculation procedure described in Sec. V is applied to Eq. (27) under condition (28). As a result, the dependences of Fig. 9 are modified at small  $\tau$ . Figure 10 illustrates the dependences  $\alpha(\tau)$  calculated with Eq. (27) at different  $A_0$  and  $\alpha_0$ .

If the function  $\alpha(\tau)$  is built, then  $\rho(x, \tau)$  is determined and the potential distribution  $\varphi(x, z, \tau)$  can be calculated as<sup>80</sup>

$$\varphi(x, z, \tau) = \int_{-\infty}^{\infty} dx' \frac{\rho(x', \tau)}{[(x - x')^2 + z^2]^{1/2}}, \quad (29)$$

where  $\rho(x, \tau)$  is the distribution (12) calculated with  $A(\tau) = A_0 = \text{const}$  and  $\alpha(\tau)$  determined from Eq. (27). Figure 11(a) illustrates the potential difference  $\Delta\varphi(\tau)$  between the spatial points with coordinates  $(x=2l_0, z=2l_0)$  and  $(x=0, z=0)$  for  $A_0=1.0$  and  $\alpha_0=0.75$  at different  $\gamma$ .

Experimentally, the value measured directly by an electric antenna is not the potential  $\varphi(x, z, \tau)$  but the displacement current proportional to the time derivative  $\partial\varphi/\partial\tau$ . Figure 11(b) presents the set of the time dependences of  $\partial\varphi/\partial\tau$  calculated from the curves of Fig. 11(a).

## VII. DISCUSSION

Let us compare the obtained theoretical results with the experimentally observed electromagnetic emission of Sec. II. The inset in Fig. 7 shows the measured form of an individual electric pulse from a typical sequence of EME data. As was noted in Sec. II B the short-time measured signal is distorted by the system of amplifiers, filters, and transformers with

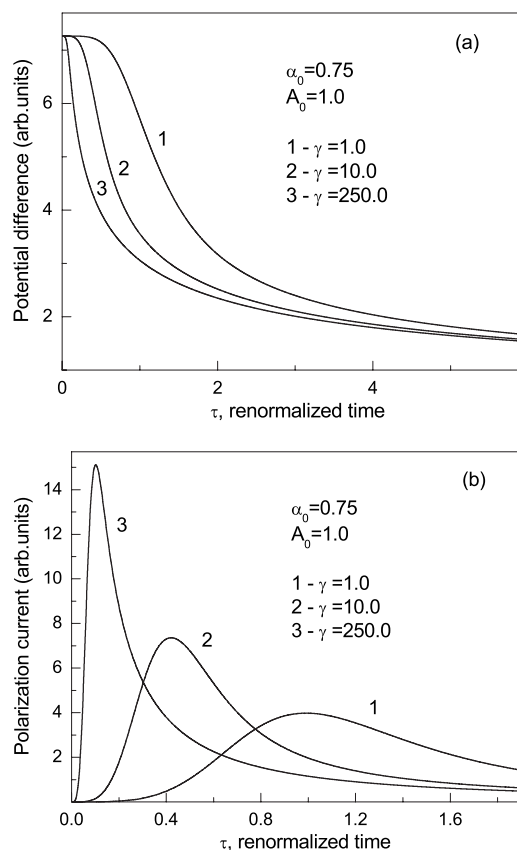


FIG. 11. Calculated form of the electric pulse. The potential difference (a) is determined between spatial points ( $x=2l_0$ ,  $z=2l_0$ ) and ( $x=0$ ,  $z=0$ ), and (b) is the time derivative  $\partial\phi/\partial\tau$ .

finite bandpass and relaxation times. In view of these experimental restrictions and the qualitative character of the proposed theoretical model neither the front of the measured pulse nor its tail can be fitted perfectly by the theoretical dependence  $\partial\phi/\partial\tau$  from Fig. 11(b). Nevertheless, an important estimation can be made on the basis of our results. Let us take into account that the initial burst of the experimentally observed pulse must have about the same time duration as the real charge relaxation process that created this pulse. The theoretical curve  $\partial\phi/\partial\tau$  can be brought into coincidence with the initial part of the experimental pulse by rescaling of the time axis (see Fig. 12). As a result, we find the corresponding conversion factor  $B/2$  between  $t$  and  $\tau$ , according to definition (10). In this case,  $B$  is the friction coefficient entering equation of motion (7) for the density of the vacancy subsystem. From Fig. 12 and Eq. (10) it follows that  $B \approx 0.9 \times 10^{-5} \text{ cm}^{-1} \text{ s}^{-1}$ . This value is in good agreement with the corresponding coefficient of dislocation friction in ionic crystals<sup>81</sup> ( $B \sim 10^{-5} - 10^{-6} \text{ g cm}^{-1} \text{ s}^{-1}$ ). This is not surprising, because it is the interaction between the defects of an atomic size (vacancies or dislocation core) and phonons that is responsible for the dynamic friction of both vacancies and dislocations in the lattice. Note that in the present case the analogy with dislocation is quite correct because the one-dimensional vacancy system studied in our model [see Eq. (7)] is, in essence, a linear (along the  $y$  axis) vacancy chain

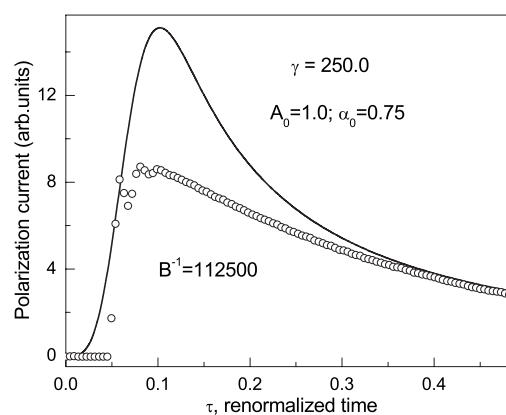


FIG. 12. Comparison between the theory and experiment. The experimental curve from the inset of Fig. 7 (scattered points) is rescaled to be fitted to the theoretical curves of Fig. 11 (see text).

quite similar to the edge of the extra plane belonging to an edge dislocation.

Thus, it seems well grounded that the formation of EME in ionic crystals during plastic deformation is due to the following two stages. In the first stage there appears an electric polarization<sup>18,19</sup> caused by a “sweeping-up” of the charged vacancies by mobile dislocations. The polarization grows up relatively slow during the formation, promotion, and locking-up of individual slip planes under easy glide and work hardening. The second stage is the “intrinsic discharge” of a “dislocation capacitor” when locked dislocation pileups burst through their stoppers and quickly lose their bound charge whose relaxation is realized through transient polarization currents. These quickly varying currents produce electric pulses observed in the experiment.

In favor of our model are also the results of the integrated EME measured on  $\gamma$ -irradiated LiF monocrystals.<sup>63</sup> It is known that the irradiation produces a lot of lattice defects which are stoppers for the dislocation glide, so the stronger irradiation dose applied, the less mobile dislocations are under an external stress. The irradiated crystals become less plastic but more brittle, and after strong enough irradiation they demonstrate only a brittle fracture instead of plastic flow. Experiments for the detection of polarization currents and EME on deformed LiF crystals exposed to  $\gamma$  doses of 10 Mrad show that there is no electromagnetic emission up to the stage of destruction when the brittle cracking occurs. This means that only mobile dislocations are able to produce the non-equilibrium charge distribution in the ionic lattice, which is the cause of macroscopic polarization currents generating the electromagnetic signals.

## VIII. CONCLUSIONS

Our experiments show the strong correlation between acoustic and electromagnetic emissions during plastic deformation of LiF monocrystals which is evidence of a common mechanism for both phenomena. The plausible reason for the electromagnetic emission under loading can be found in mechanisms of interaction between mobile dislocations and

“quasifree” charge carriers, which in the case of ionic crystals are charged vacancies. The dislocation-vacancy and dislocation-impurity interaction mechanisms as a basis for EME formation in ionic crystals are supported, among others, by the fact that the strongest electromagnetic response during plastic deformation is observed just in LiF crystals with a relatively high yield point [as compared to NaCl and KCl whose yield points are 5 times lower than in LiF (Ref. 70)]. In the future, this fact will be tested in more details by AE and EME measurements on different ionic crystals with various content of impurities of foreign valence.

The investigation of EME mechanisms makes it possible to observe new physical effects caused by delicate features of electromagnetic processes associated with deformation and destruction of both crystalline and noncrystalline solids. Progress in this area will advance the EME method as an effective tool for the diagnostics and control of materials. There is good reason to believe that electromagnetic methods will have an advantage over conventional acoustic emission.

Indeed, the registered electromagnetic image of an elementary deformation event is quite well determined as compared to the corresponding AE pulse which is usually masked by a noiselike acoustic “tail” formed due to the contribution of intrinsic acoustic modes of a finite-sized sample. The finite-sized solid is an “acoustic filter” with a complicated set of eigenmodes (Rayleigh-Lamb and shear waves). So the acoustic response of the sample on a deformation event is an intricate mixture of eigenmodes, which makes it difficult to extract constructive information on this event. On the contrary, EME holds practically nondistorted information about the primordial deformation processes that are sources of the corresponding electromagnetic signals.

#### ACKNOWLEDGMENTS

We acknowledge support from NATO Grant No. CBP-.NUKR.EV.981312 and support from Kapodistrias Project, National and Kapodistrian University of Athens.

\*vhadjico@phys.uoa.gr

- <sup>1</sup>V. S. Boiko, R. I. Garber, L. F. Krivenko, and S. S. Krivula, *Sov. Phys. Solid State* **11**, 3041 (1970).
- <sup>2</sup>V. S. Boiko, R. I. Garber, V. F. Kivshik, and L. F. Krivenko, *Sov. Phys. JETP* **44**, 372 (1976).
- <sup>3</sup>J. Baram and J. Rosen, *Acta Metall.* **30**, 655 (1981).
- <sup>4</sup>K. A. Chishko, *Sov. Phys. Solid State* **31**, 476 (1989).
- <sup>5</sup>K. A. Chishko, *Sov. Phys. Solid State* **34**, 462 (1992).
- <sup>6</sup>K. A. Chishko, *Sov. Phys. Acoust.* **36**, 84 (1990).
- <sup>7</sup>K. A. Chishko, *Phys. Solid State* **36**, 1169 (1994).
- <sup>8</sup>D. R. James and S. N. Carpenter, *J. Appl. Phys.* **42**, 4685 (1971).
- <sup>9</sup>V. S. Boiko and L. F. Krivenko, *Sov. Phys. JETP* **53**, 129 (1981).
- <sup>10</sup>V. S. Boiko and L. F. Krivenko, *Sov. Phys. Solid State* **30**, 410 (1988).
- <sup>11</sup>Ll. Mañosa, A. Planes, D. Rouby, and J. L. MacQueron, *Acta Metall. Mater.* **38**, 1635 (1990).
- <sup>12</sup>T. N. Antsygina and K. A. Chishko, *Phys. Solid State* **35**, 898 (1993).
- <sup>13</sup>A. M. Kosevich, *Sov. Phys. Usp.* **7**, 837 (1964).
- <sup>14</sup>A. M. Kosevich, *Dislocations in the Theory of Elasticity* (Naukova Dumka, Kiev, 1978) (in Russian).
- <sup>15</sup>G. Stenzel, *Phys. Status Solidi* **34**, 351 (1969).
- <sup>16</sup>A. V. Stepanov, *Phys. Z. Sowjetunion* **4**, 609 (1933).
- <sup>17</sup>A. V. Stepanov, *Z. Phys.* **81**, 560 (1933).
- <sup>18</sup>R. W. Whitworth, *Adv. Phys.* **24**, 203 (1975).
- <sup>19</sup>R. W. Whitworth, *Philos. Mag.* **15**, 305 (1967).
- <sup>20</sup>A. Huddart and R. W. Whitworth, *Philos. Mag.* **27**, 107 (1973).
- <sup>21</sup>R. M. Turner and R. W. Whitworth, *Philos. Mag.* **21**, 1187 (1970).
- <sup>22</sup>R. W. Davidge, *Philos. Mag.* **8**, 1369 (1963).
- <sup>23</sup>R. W. Davidge, *J. Phys. Chem. Solids* **25**, 907 (1964).
- <sup>24</sup>G. Remault, J. Vennik, and S. Amelinckx, *J. Phys. Chem. Solids* **16**, 158 (1960).
- <sup>25</sup>T. Yoshi-yama, M. Mannami, and K. Tanaka, *J. Phys. Soc. Jpn.* **24**, 1019 (1968).
- <sup>26</sup>E. Van Dingenen, *Philos. Mag.* **31**, 1263 (1975).
- <sup>27</sup>R. W. Whitworth, *Philos. Mag.* **5**, 425 (1960).
- <sup>28</sup>L. M. Belyaev, V. V. Nabatov, and Yu. N. Martyshev, *Sov. Phys. Crystallogr.* **7**, 464 (1962).
- <sup>29</sup>Yu. N. Martyshev, *Sov. Phys. Crystallogr.* **10**, 167 (1965).
- <sup>30</sup>R. Sh. Kil'keev and V. S. Kuksenko, *Sov. Phys. Solid State* **22**, 1829 (1980).
- <sup>31</sup>N. G. Politov, M. V. Galustashvili, and I. M. Paperno, *Sov. Phys. Solid State* **12**, 2421 (1970).
- <sup>32</sup>A. A. Urusovskaya, *Sov. Phys. Usp.* **11**, 631 (1968).
- <sup>33</sup>M. I. Kornfel'd, *Sov. Phys. Usp.* **18**, 459 (1975).
- <sup>34</sup>V. M. Finkel', Yu. I. Tyalin, Yu. I. Golovin, L. N. Muratova, and M. V. Gorshenev, *Sov. Phys. Solid State* **17**, 1116 (1979).
- <sup>35</sup>V. M. Finkel', Yu. I. Golovin, V. E. Sereda, G. P. Kulikova, and L. B. Zuev, *Sov. Phys. Solid State* **17**, 492 (1979).
- <sup>36</sup>F. Fröhlich and D. Suisly, *Phys. Status Solidi* **4**, 151 (1964).
- <sup>37</sup>D. B. Fischbach and A. S. Nowick, *Phys. Rev.* **99**, 1333 (1955).
- <sup>38</sup>D. B. Fischbach and A. S. Nowick, *J. Phys. Chem. Solids* **5**, 302 (1958).
- <sup>39</sup>R. W. Whitworth, *Philos. Mag.* **10**, 801 (1964).
- <sup>40</sup>P. Varotsos and K. Alexopoulos, *Tectonophysics* **110**, 73 (1984); **110**, 99 (1984).
- <sup>41</sup>P. Varotsos, K. Alexopoulos, K. Nomikos, and M. Lazaridou, *Tectonophysics* **152**, 193 (1988).
- <sup>42</sup>P. Varotsos, N. Sarlis, and M. Lazaridou, *Phys. Rev. B* **59**, 24 (1999).
- <sup>43</sup>N. Sarlis, M. Lazaridou, P. Kaporis, and P. Varotsos, *Geophys. Res. Lett.* **26**, 3245 (1999).
- <sup>44</sup>Yu. I. Golovin, T. P. D'yachek, V. I. Uskov, and A. A. Shibkov, *Sov. Phys. Solid State* **27**, 344 (1985).
- <sup>45</sup>Yu. I. Golovin and A. A. Shibkov, *Sov. Phys. Solid State* **28**, 1964 (1986).
- <sup>46</sup>Yu. I. Golovin, T. P. D'yachek, V. I. Orlov, and Yu. I. Tyalin, *Sov. Phys. Solid State* **27**, 671 (1985).
- <sup>47</sup>C. Mavromatou and V. Hadjicontis, in *Earthquake Thermodynamics and Phase Transformations in the Earth's Interior*, edited by R. Teisseyre and E. Majewski (Academic Press, San

- Diego, 2001), Chap. 21, pp. 501–517.
- <sup>48</sup>D. Ninos, G. S. Tombras, C. Mavromatou, and V. Hadjicontis, *IEEE Geosci. Remote Sensing Lett.* **1** (3), 162 (2004).
- <sup>49</sup>C. Mavromatou, V. Hadjicontis, D. Ninos, D. Mastrogiannis, E. Hadjicontis, and K. Eftaxias, *Phys. Chem. Earth* **29**, 353 (2004).
- <sup>50</sup>V. Hadjicontis, C. Mavromatou, and D. Ninos, *Nat. Hazards Earth Syst. Sci.* **4**, 633 (2004).
- <sup>51</sup>M. Born and K. Huang, *Dynamical Theory of Crystal Lattices* (Clarendon Press, Oxford, 1954).
- <sup>52</sup>G. Leibfried, *Gittertheorie der mechanischen und thermischen Eigenschaften der Kristalle* (Springer-Verlag, Berlin, 1955).
- <sup>53</sup>V. M. Kontorovich, *Sov. Phys. Usp.* **27**, 134 (1984).
- <sup>54</sup>M. I. Kaganov, V. Ya. Kravchenko, and V. D. Natsik, *Sov. Phys. Usp.* **16**, 878 (1974).
- <sup>55</sup>V. I. Al'shits, E. V. Darinskaya, and O. L. Kazakova, *Phys. Solid State* **40**, 70 (1998).
- <sup>56</sup>V. I. Al'shits, E. V. Darinskaya, I. V. Gektina, and F. F. Lavrent'ev, *Sov. Phys. Crystallogr.* **35**, 597 (1990).
- <sup>57</sup>M. I. Molotskii, *Sov. Phys. Solid State* **33**, 1760 (1991).
- <sup>58</sup>K. A. Chishko, *Sov. Phys. Acoust.* **35**, 310 (1989).
- <sup>59</sup>O. V. Charkina and K. A. Chishko, *Phys. Solid State* **43**, 1898 (2001).
- <sup>60</sup>Yu. I. Golovin and V. I. Orlov, *Sov. Phys. Solid State* **30**, 2489 (1988).
- <sup>61</sup>V. Hadjicontis and C. Mavromatou, *Geophys. Res. Lett.* **21**, 1687 (1994).
- <sup>62</sup>V. Hadjicontis, G. S. Tombras, D. Ninos, and C. Mavromatou, *IEEE Geosci. Remote Sensing Lett.* **2** (2), 118 (2005).
- <sup>63</sup>V. Hadjicontis, C. Mavromatou, and Y. Enomoto, *Mater. Sci. Forum* **239-241**, 435 (1997).
- <sup>64</sup>P. Varotsos, N. Sarlis, and M. Lazaridou, *Phys. Rev. B* **59**, 24 (1999).
- <sup>65</sup>P. Varotsos, V. Hadjicontis, and A. S. Nowick, *Acta Geophys. Pol.* **49**, 415 (2001).
- <sup>66</sup>P. Varotsos, K. Eftaxias, F. Vallianatos, and M. Lazaridou, *Geophys. Res. Lett.* **23**, 1295 (1996).
- <sup>67</sup>K. Eftaxias, P. Kaporis, E. Dologlou, J. Kopanas, N. Bogris, G. Antonopoulos, A. Peratzakis, and V. Hadjicontis, *Geophys. Res. Lett.* **29**, 69 (2002).
- <sup>68</sup>Y. F. Contoyiannis, P. G. Kaporis, and K. A. Eftaxias, *Phys. Rev. E* **71**, 066123 (2005).
- <sup>69</sup>W. G. Johnston, *J. Appl. Phys.* **33**, 2716 (1962).
- <sup>70</sup>B. I. Smirnov, *Dislocation Structure and Work Hardening in Crystals* (Nauka, Leningrad, 1981). (in Russian).
- <sup>71</sup>V. Hadjicontis, V. E. Panin, Ye. Ye. Deryugin, D. Ninos, C. Mavromatou, and K. Eftaxias, *Phys. Mesomech.* **7**, 71 (2004).
- <sup>72</sup>V. E. Panin, Ye. Ye. Deryugin, V. Hadjicontis, C. Mavromatou, and K. Eftaxias, *Phys. Mesomech.* **4**, 21 (2001).
- <sup>73</sup>The quantity  $\sigma_0 \sim 6.0$  MPa in Refs. [71](#) and [72](#) is the absolute value of the applied stress which is twice as large as the resolved shear stress for the given slip geometry.
- <sup>74</sup>K. A. Chishko, *Acoust. Phys.* **39**, 80 (1993).
- <sup>75</sup>J. P. Hirth and J. Lothe, *Theory of Dislocations* (McGraw-Hill, New York, 1970).
- <sup>76</sup>We use here the same symbol  $\rho$  to denote the three-, two-, and one-dimensional distributions, but with different sets of arguments [ $\rho(\mathbf{r}, t)$ ,  $\rho(x, z, t)$ , and  $\rho(x, t)$ , respectively].
- <sup>77</sup>A. Lidiard, *Ionic Conductivity* (Springer-Verlag, Berlin, 1957).
- <sup>78</sup>V. D. Natsik and K. A. Chishko, *Sov. Phys. Solid State* **17**, 214 (1975).
- <sup>79</sup>L. E. Elsholts, *Differential Equations* (Hindustan, Delhi, 1961).
- <sup>80</sup>W. K. H. Panofsky and M. Phillips, *Classical Electricity and Magnetism* (Addison-Wesley, Reading, MA, 1959).
- <sup>81</sup>W. Mason, *J. Acoust. Soc. Am.* **32**, 458 (1960).